Asian Journal of Chemistry; Vol. 32, No. 12 (2020), 3165-3172

ASIAN JOURNAL OF CHEMISTRY

https://doi.org/10.14233/ajchem.2020.22965

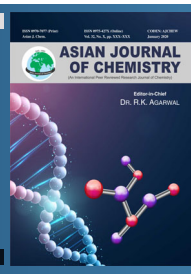

Structural, Thermal, Electrical and Dielectric Properties of $La_{1-x}Sr_xMn_{0.50}Fe_{0.50}O_3$ {0.10 ≤ x ≤ 0.40} Cathode Material for Solid Oxide Fuel Cells

MANOKAMNA[1,*], S. PAUL[1], A. SINGH[2], K.L. SINGH[3] and A.P. SINGH[1]

[1]Department of Applied Sciences, I.K. Gujral Punjab Technical University, Jalandhar-144001, India
[2]Department of Physics, Guru Nanak Dev University, Amritsar-143005, India
[3]Department of Applied Sciences, DAV Institute of Engineering and Technology, Jalandhar-144001, India

*Corresponding author: E-mail: manokamna12333@gmail.com

Received: 31 August 2020; *Accepted*: 7 October 2020; *Published online*: 7 December 2020; AJC-20156

$La_{1-x}Sr_xMn_{0.50}Fe_{0.50}O_3$ {0.10 ≤ x ≤ 0.40} perovskite ceramics material is prepared by solid-state reaction method and samples are characterized to study their structural, thermal, electrical and dielectric properties. X-ray diffraction results show that as prepared samples are well crystallized in single phase and have rhombohedral crystal structure. Density is measured by Archimedes principle and with Sr substitution its value decreasing. Thermogravimetric analysis shows the weight gain in the material above 300 ºC. Thermal expansion coefficient value for x = 0.10 and 0.40 composition is found to be 12.9×10^{-6} ºC^{-1} and 11.3×10^{-6} ºC^{-1}, respectively upto 800 ºC. Impedance analyzer is used to study dielectric and electrical properties which show that all the as prepared samples obey non-Debye relaxation behaviour. The maximum conductivity value is 121.09 S cm^{-1} for x = 0.10 and 155.96 S cm^{-1} for x = 0.40 at 600 ºC and 303.59 S cm^{-1} for x = 0.10 and 362.35 S cm^{-1} for x = 0.40 at 800 ºC which confirmed that in the experimental perovskite the conductivity increases after Sr doping . Activation energy also found to be decreases with Sr substitution. Therefore, studied properties confirmed that the as-prepared material is a suitable cathode material for intermediate temperature solid oxide fuel cells (SOFCs).

Keywords: Solid oxide fuel cells, Cathode material, Stronium, Impedance spectroscopy, Conductivity.

INTRODUCTION

The reduction of resources of fossil fuel makes it a necessity to discover sustainable as well as clean alternative energy sources. One of such alternative forthcoming generation energy carriers is hydrogen which is portable, clean and renewable [1,2]. Solid oxide fuel cells (SOFCs) are well known sources of production of hydrogen and one of the striking alternative energy sources because of its comparatively high efficiency, inexpensiveness and low sensitivity to impurities [3-7]. The efficiency of solid oxide fuel cells is approximately 60% and can reach up to 80% if total heat recovered in the cell [8]. Material of component of SOFCs plays an important role to reach at this high efficiency, however certain issues arise which limit the effectiveness of cathode materials such as lowering the operating temperature and mismatching of thermal expansion coefficient with another components result in to fall in the conductivity and degredation of the material, which further affect the performance of the cell [8-11]. To attain desired efficiency, cathode material of SOFCs must have high electronic conductivity (larger than 100 S cm^{-1}), large catalytic activities, chemical compatibility with other components, sufficient porosity and low cost [4]. There is a number of perovskite cathode materials like $LaMnO_3$, $LaFeO_3$ and $LaCoO_3$ with appropriate ion doping, recommended and used as cathode materials in SOFCs as reported earlier [12]. Size of strontium is comparable to lanthanum, hence strontium is generally used as dopant in $LaMnO_3$ which increases the concentration of electrons and holes in $La_{1-x}Sr_xMnO_{3\pm\delta}$ ($x \leq 0.80$) (LSM) and lift up the electrical conductivity [13]. However, on lowering the operating temperature LSM show high value of polarization resistance and activation energy (E_a) which further fall the SOFC performance [14]. Strontium modified $LaFeO_3$ (LSF) is also reported as promising cathode material for SOFCs. Substitution of Sr in $LaFeO_3$ produce charge imbalance, which further compensated either by formation of Fe^{4+} ion or by creation of oxygen vacancy

and therefore increase the conductivity [15-17]. The flexibility of perovskite material to the transition and alkali earth metals provides a huge composition range for challenging targets. Therefore, in this work, Sr^{2+} is substituted at lanthanum site of $LaMnFeO_3$, which create the charge imbalance and charge neutrality is compensated by reduction or oxidation of Mn and Fe consequently increase the conductivity.

EXPERIMENTAL

Synthesis: $La_{1-x}Sr_xMn_{0.50}Fe_{0.50}O_3$ $\{0.10 \le x \le 0.40\}$ perovskite are synthesized by solid state reaction method. Samples were prepared by using raw materials strontium carbonate ($SrCO_3$), manganese oxide (MnO), ferric oxide (Fe_2O_3) and lanthanum oxide (La_2O_3). All the raw powders were procured from Sigma-Aldrich and 99.9% pure. Raw powders were taken in stoichiometric ratio and ball milled for 6 h by using zirconia oxide balls. Ball milled powder was then mixed further for 2 h with the help of agate mortar and pestle. Precursor was calcined at 1200 ºC for 12 h and then polyvinyl alcohol (PVA) 2 wt % was mixed. Hydraulic pressure was used to make pellets which further sintered at 1400 ºC for 2 h. Sintered samples were further characterized for study the structural, thermal, electrical and dielectric properties.

RESULTS AND DISCUSSION

XRD studies: Structural properties of the prepared samples were studied with the help of X-ray diffractometer. The wavelength,temperature range, step size and scan rate are 1.54 Å, 20-80 ºC, 0.02 and 2º/min, respectively. Obtained X-Ray patterns are shown in Fig. 1,while the XRD data is analyzed using X'Pert High Score Plus software.

High intense as well as sharp peaks confirm the crystalline nature of the samples. The data shows that the crystal structure is rhombohedral, space group R-3c and group no. 167. No peak in XRD pattern is left unassigned, which confirmed that the prepared samples are crystallized in a single phase. Variation of occupied volume, specific free volume and crystallographic lattice parameters with Sr substitution of the prepared crystalline material is shown in Table-1. It is observed that lattice parameters and unit cell volume decreasing with replacement of La by Sr in all the samples but actually unit cell volume must increase since ionic radii of Sr^{2+} is larger than La^{3+}. But it is not so and this contradiction is arise due to creation of charge imbalance on substitution of Sr , which further compensated by (i) conversion of $Mn^{3+}/(Fe^{2+}/Fe^{3+})$ into Mn^{4+}/Fe^{4+} (ii) by creation of oxygen vacancies in the materials. Ionic radii of Mn^{4+}/Fe^{4+} smaller than $Mn^{3+}/(Fe^{2+}/Fe^{3+})$, which cause a decrease of unit cell volume. Therefore, it may be probable that in LSMF system, Mn^{4+} have small ionic radii influences the system much powerfully as compared to Sr^{2+} have larger ionic radii. Also, as said by Pauling's rule, Mn-O bonds are more strengthen by Mn^{4+} ions, which can also decrease the unit cell volume [18].

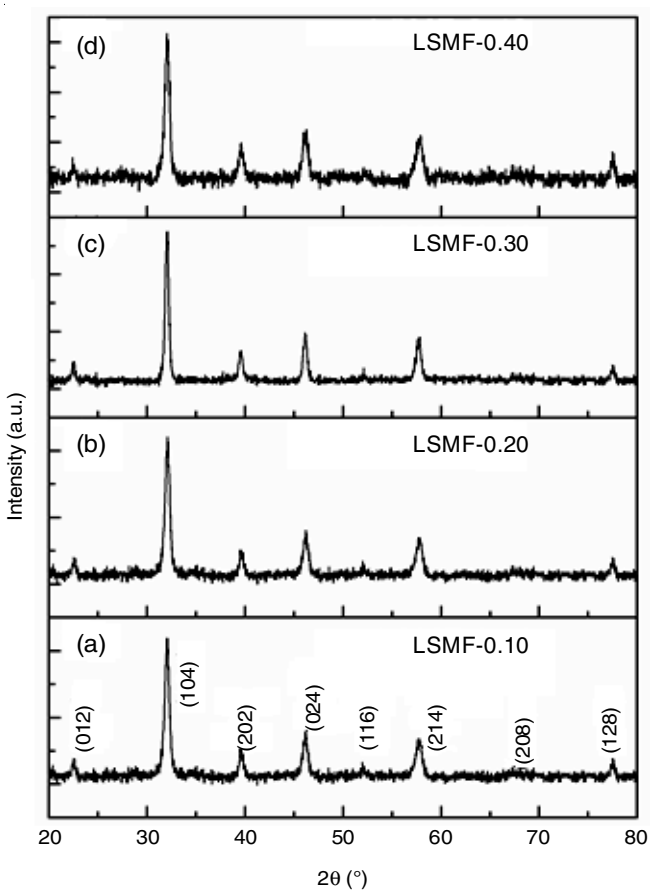

Fig. 1. XRD pattern of rhombohedral $La_{1-x}Sr_xMn_{0.50}Fe_{0.50}O_3$ $(0.10 \le x \le 0.40)$ solid solutions

SEM studies: Morphologies of the grains of samples can sturdily affect the net conductivity of the materials. Surface morphology of the prepared samples were studied by using scanning electron microscope (SEM) Carl Zeiss Supra 55, Germany. Micrographs (Fig. 2) clearly show that grains are well attached to each other, which confirm the samples are well sintered and obtained grains are non-uniform, randomly oriented and with the Sr substitution the average size of grains are decreasing. It is reported in literature that with substitution of alkaline earth metals leads to suppress the necking of grains because of reduced mobility of grain boundary and therefore reduce the grain size [19].

TABLE-1
LATTICE PARAMETERS AND VOLUME OF $La_{1-x}Sr_xMn_{0.50}Fe_{0.50}O_3$ $(0.10 \le x \le 0.40)$

Composition	Lattice parameters		Ratio c/a	Cell volume (Å^3)	Occupied volume	Specific free volume
	a (Å)	c (Å)				
$La_{0.90}Sr_{0.10}$ $Mn_{0.50}Fe_{0.50}O_3$	5.512	13.356	2.423	351.408	40.880	0.883
$La_{0.80}Sr_{0.20}$ $Mn_{0.50}Fe_{0.50}O_3$	5.492	13.354	2.431	348.811	41.108	0.882
$La_{0.70}Sr_{0.30}$ $Mn_{0.50}Fe_{0.50}O_3$	5.493	13.351	2.430	348.859	41.336	0.881
$La_{0.60}Sr_{0.40}$ $Mn_{0.50}Fe_{0.50}O_3$	5.490	13.349	2.431	348.426	41.564	0.880

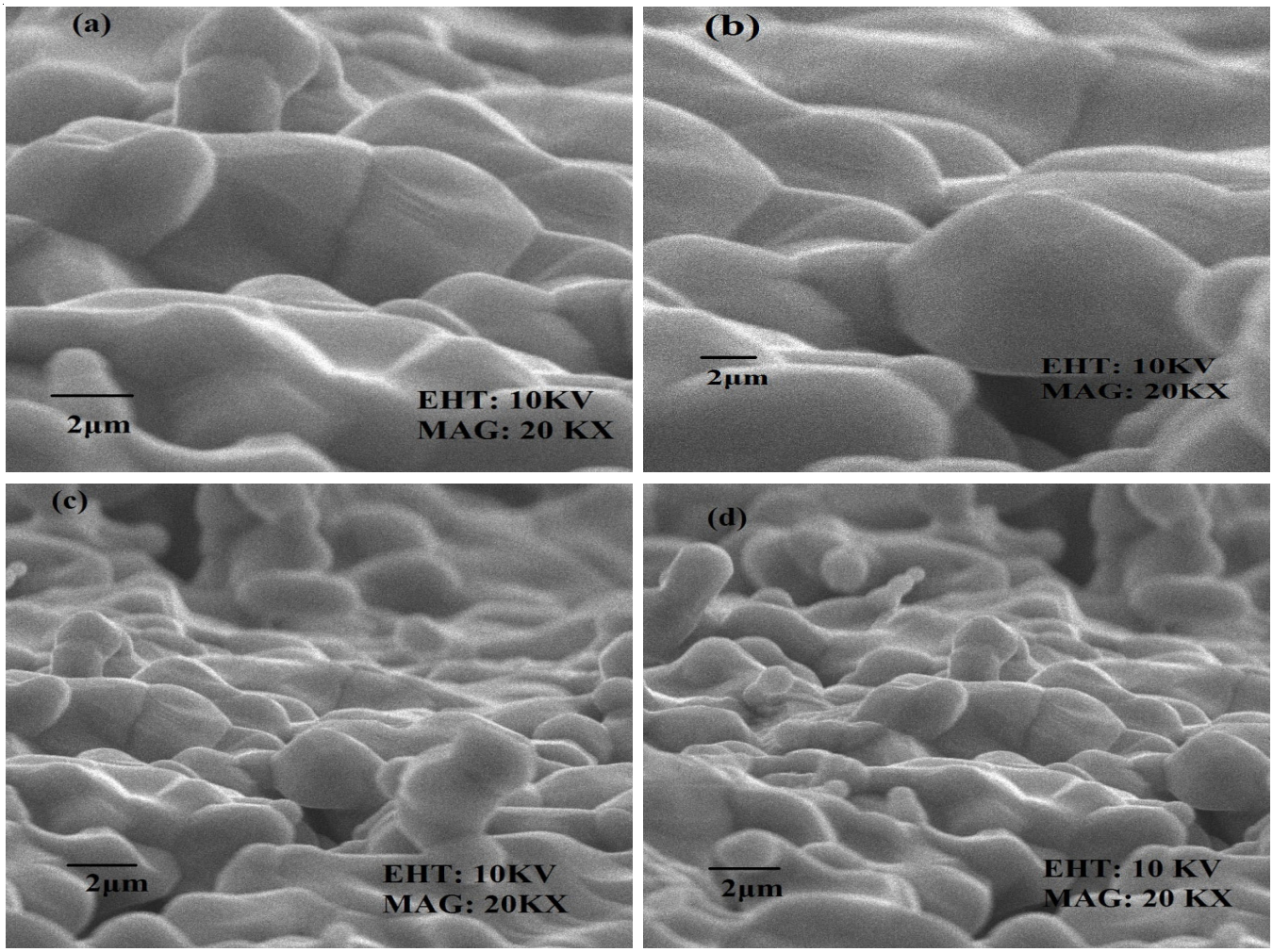

Fig. 2. Micrographs of $La_{1-x}Sr_xMn_{0.50}Fe_{0.50}O_3$ ($0.10 \le x \le 0.40$) solid solutions

Density: Archimedes liquid displacement method is used to find out the experimental density and theoretical density is calculated by the use of following formula.

$$\rho = \frac{W_a}{W_a - W_l} \times \rho_{liquid}$$

where W_l is weight of pellet in liquid and W_a is weight of pellet in air; ρ is density of pellet and ρ_{liquid} is the density of the liquid used. Density value of the pellets decrease with Sr modification (Table-2). The SEM images and calculated density values of samples are found to be in well agreement.

Thermogravimetric analysis: Thermogravimetric analysis explains the effect of temperature variation on the weight change during sintering of the samples. The TGA curves of prepared pellet are obtained in the air atmosphere at 25 ºC to 800 ºC, at the heating rate of 5 ºC/min and the reference material used was Al_2O_3 powder. Thermogravimetric analysis graphs of $La_{0.7}Sr_{0.3}Fe_xMn_{1-x}O_3$ ceramic solid solutions with (a) $_x$ = 0.10 and (b) $_x$ = 0.40 are shown in Fig. 3. From the TGA curves, it is observed that in the beginning, a sharp weight loss in the material up to 300 ºC. These kinds of weight loss in the prepared material arise because of loss of moisture content present in the pellets in addition to transform of carbonate on heating into oxide. Beyond 300 ºC and above, weight gain begin in the material. It is well reported in literature that this weight change in the material aries because of charge imbalance created on Sr substitution at A side and Fe at B site in $LaMnO_3$ perovskite. Replacement become the cause of reduction of Mn^{4+}/Fe^{4+} into

TABLE-2
DENSITY, AVERAGE GRAIN SIZE AND TOLERANCE FACTOR OF $La_{1-x}Sr_xMn_{0.50}Fe_{0.50}O_3$ ($0.10 \le x \le 0.40$)

Composition	Density			Average grain size (μm)	Standard deviation	Tolerance factor
	Theoretical density (d_{th}) (g cm^{-3})	Experimental density (d) (g cm^{-3})	(d/d_{th}) (%)			
$La_{0.90}Sr_{0.10}Mn_{0.50}Fe_{0.50}O_3$	5.78	5.13	88.76	2.41	0.94	0.727
$La_{0.80}Sr_{0.20}Mn_{0.50}Fe_{0.50}O_3$	5.62	5.04	89.68	2.16	0.63	0.728
$La_{0.70}Sr_{0.30}Mn_{0.50}Fe_{0.50}O_3$	5.47	4.97	90.86	1.63	0.55	0.729
$La_{0.60}Sr_{0.40}Mn_{0.50}Fe_{0.50}O_3$	5.31	4.86	91.53	1.17	0.29	0.729

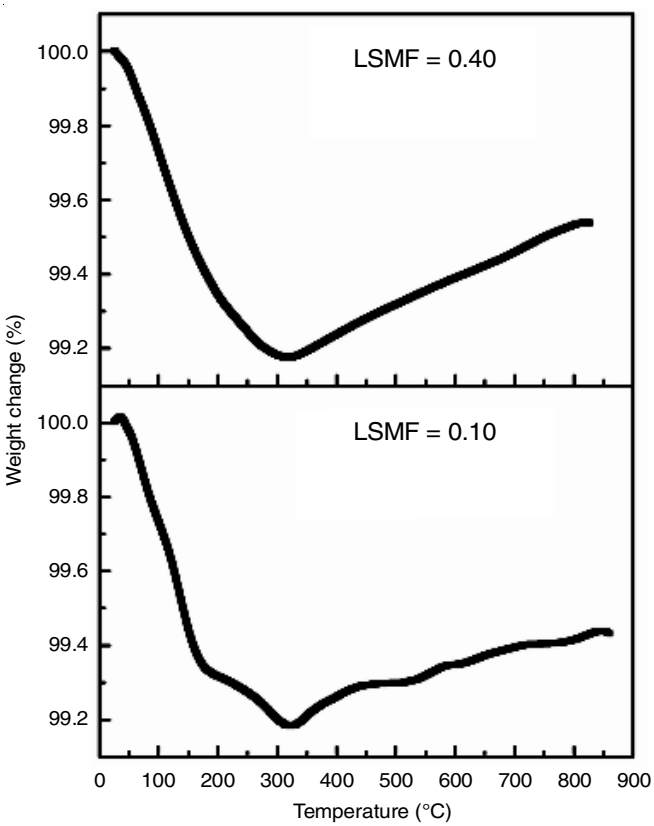

Fig. 3. Thermal graph of $La_{1-x}Sr_xMn_{0.50}Fe_{0.50}O_3$ ($x = 0.10$ and 0.40) solid solutions

$Mn^{3+}/(Fe^{2+}/Fe^{3+})$ creates oxygen vacancies or the oxidation of $Mn^{3+}/(Fe^{2+}/Fe^{3+})$ into Mn^{4+}/Fe^{4+}, which cause annihilation of oxide vacancies inside the bulk material [20,21]. Also, it is clearly visible that percentage weight gain in $x = 0.40$ is comparably more than the $x = 0.10$, which indicated that prepared material achieved more stability upon Sr substitution.

Thermal expansion coefficient: Material exhibits higher value of thermal expansion coefficient (TEC) becomes the cause of cracking of the electrolyte or delamination at interface of cathode/electrolyte lead to fall the cell performance [22]. In addition, discrepancy of TEC with other component (anode and electrolyte) creates thermal stress and reduce the cell performance. The TEC curves of samples $x = 0.10$ and 0.40 up to 800 ºC are shown in Fig. 4.

TEC graphs of $La_{1-x}Sr_xMn_{0.50}Fe_{0.50}O_3$ ($x = 0.10$ and 0.40) solid solutions upto 800 °C are 12.9×10^{-6} and 11.3×10^{-6} °C^{-1}, respectively. At high value of temperature, the foremost reason of raise or fall the TEC is loss or gain of oxygen in crystal lattice and in addition to this existence of superstructure plus ordering of oxygen vacancies lead to potential energy well more symmetric because of superior ordering of oxygen vacancies inside the material [23,24]. In the present samples, oxidation of Mn and Fe may be the cause of decrease in the TEC value with Sr substitution.

Dielectric properties: Relative dielectric permittivity (ε_R) depend upon frequency, which is given by the following relation:

$$\varepsilon_R(\omega) = \varepsilon'(\omega) - i\omega\varepsilon''(\omega)$$

where ω, ε′ (ω) and ε″ (ω) are angular frequency, real part of dielectric constant and imaginary part of dielectric constant,

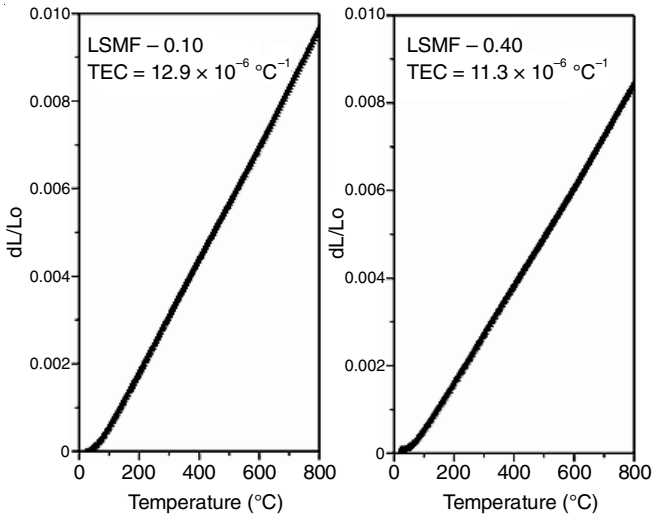

Fig. 4. Thermal expansion coefficient of $La_{1-x}Sr_xMn_{0.50}Fe_{0.50}O_3$ ($x = 0.10$ and 0.40) solid solutions

respectively. Real part of dielectric constant is in phase with the applied field whereas imaginary part is in quadrature with the applied field. Variation of ε′ and ε″ (temperature dependent) with respect to frequency at different temperature are shown in Figs. 5 and 6. Real part ε′(ω) of dielectric constant and imaginary part ε″(ω) of dielectric constant with respect to frequency curves are fitted by means of Cole-Cole model. Cole-Cole model is a relaxation model, which is generally used for the explanation of dielectric relaxations [25].

$$\varepsilon' = \varepsilon_\infty + \frac{(\varepsilon_0 - \varepsilon_\infty)\left(1 + (\omega\tau)^{(1-\alpha)}\sin\frac{\alpha\pi}{2}\right)}{\left(1 + 2(\omega\tau)^{(1-\alpha)}\sin\frac{\alpha\pi}{2} + (\omega\tau)^{2(1-\alpha)}\right)}$$

$$\varepsilon'' = \frac{(\varepsilon_0 - \varepsilon_\infty)\left((\omega\tau)^{(1-\alpha)}\cos\frac{\alpha\pi}{2}\right)}{\left(1 + 2(\omega\tau)^{(1-\alpha)}\sin\frac{\alpha\pi}{2} + (\omega\tau)^{2(1-\alpha)}\right)}$$

where exponent α, is used as parameter and represent diverse spectral shapes. If exponent α is equal to zero the relaxations are stretched, then Cole-Cole model reduces to Debye behaviour. However, if exponent α is greater than zero, Cole-Cole model stand for non-Debye behaviour. Different values of exponents α for both ε′ and ε″ (Table-3) are more than zero, which specified that the present systems exhibit non-Debye relaxation behaviour. Figs. 5 and 6 showed that in the lower frequency region both ε′ and ε″ constantly decreasing with rising the frequency for different temperature values and nearly show a linear behaviour in the higher frequency region and well explained by dipolar relaxation phenomenon [26]. There is negligible dielectric loss in the material, which is confirmed by the absence of peak in the graphs and hence polarizations are completely dominated to hopping mechanism [27]. In low frequency region, total polarization is the contribution of electronic, dipolar, ionic and space charge polarization and hence exhibit maximum value but at the higher frequency region both real part ε′ and imaginary part ε″ lag behind the switching signal of dipolar orientation,

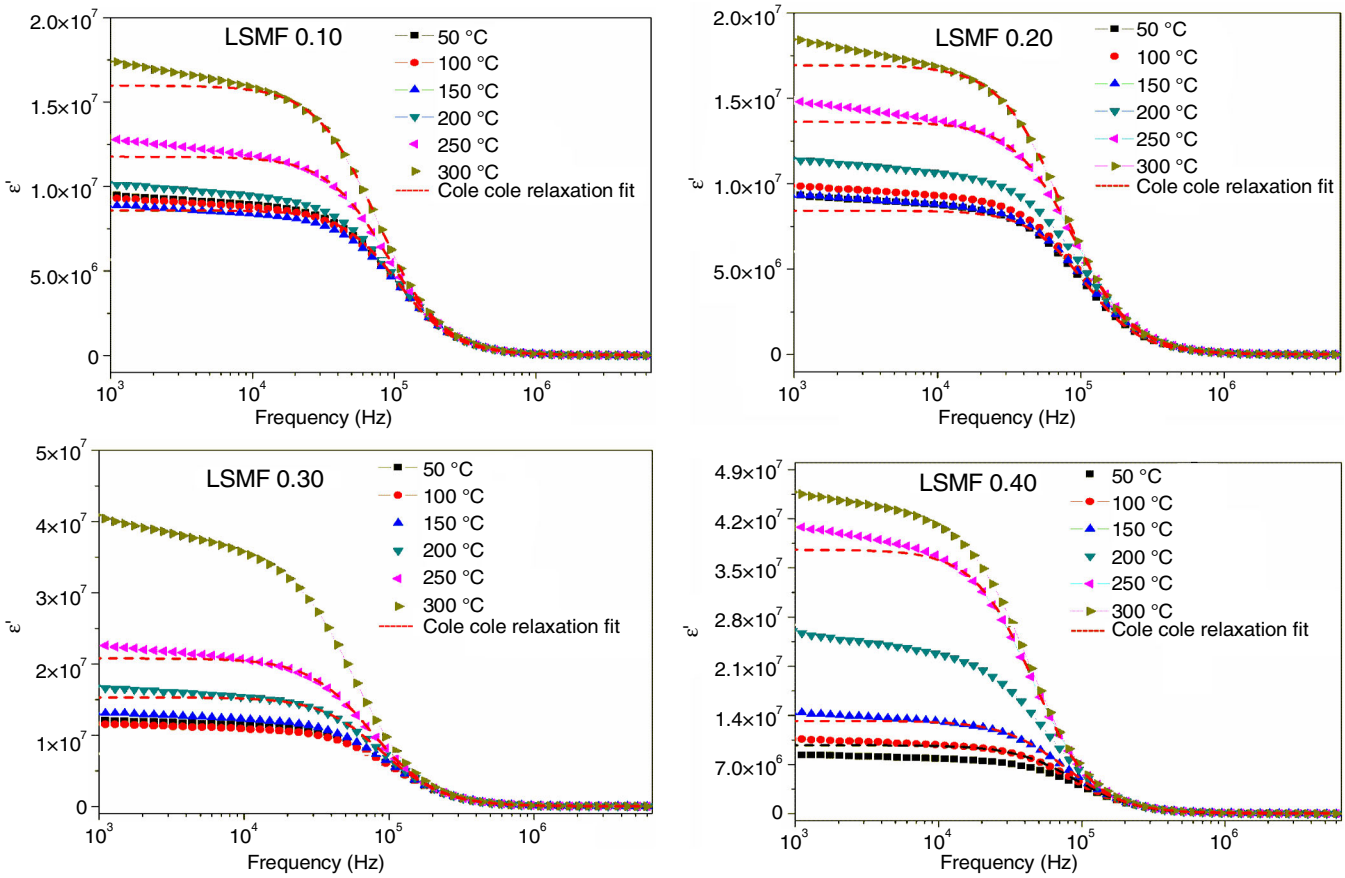

Fig. 5. Dielectric constant ε′ with respect to frequency response of $La_{1-x}Sr_xMn_{0.50}Fe_{0.50}O_3$ $(0.10 \le x \le 0.40)$ solid solutions

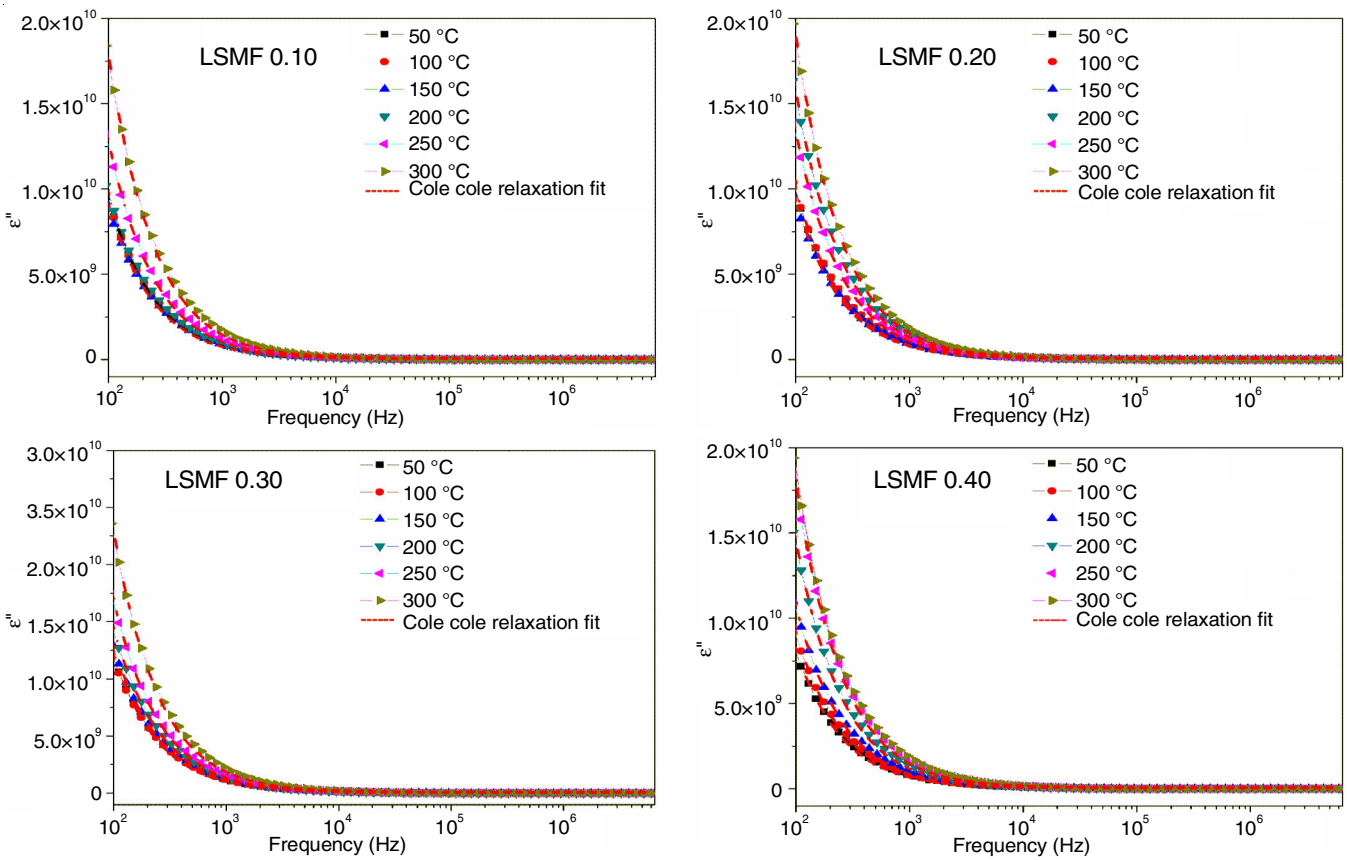

Fig. 6. Dielectric constant ε″ *vs.* frequency of $La_{1-x}Sr_xMn_{0.50}Fe_{0.50}O_3$ $(0.10 \le x \le 0.40)$ solid solutions

TABLE-3
VALUES OF α-PARAMETER AT DIFFERENT TEMPERATURE VALUE OF $La_{1-x}Sr_xMn_{0.50}Fe_{0.50}O_3$ ($0.10 \le x \le 0.40$) SOLID SOLUTIONS

Temp. (°C)	LSMF-0.10		LSMF-0.20		LSMF-0.30		LSMF-0.40	
	From ε′	From ε″	From ε′	From ε″	From ε′	From ε″	From ε′	From ε″
50	0.642	0.910	0.924	0.384	0.133	0.254	0.154	0.659
100	0.321	0.914	0.781	0.281	0.654	0.272	0.156	0.784
150	0.642	0.933	0.594	0.393	0.614	0.266	0.491	0.669
200	0.623	0.785	0.933	0.483	0.544	0.265	0.245	0.653
250	0.586	0.586	0.684	0.235	0.235	0.123	0.235	0.235
300	0.423	0.548	0.534	0.256	0.259	0.259	0.356	0.325

lead to around linear variation because some number of the polarizations are filtered out from the net polarizability and consequently diminish the polarization in this region. Additionally, grain boundary and electrode effect also play important role in the falling behaviour of dielectric constant at high frequency as reported in literature whereas Maxwell-Wagner model very well explain the behaviour of dielectric constant at low frequency region [28,29]. Also it is noticeably indicated from the curves that both ε′ and ε″ increases with Sr addition, which may not be caused by the dipolar polarization but occur because of the participation of interfacial polarization.

Impedance spectroscopy: Behaviour of real part of impedance (Z′) and imaginary part of impedance (Z″) with respect to frequency at 50 to 300 ºC for $x = 0.10$ and 0.40 samples are given in Fig. 7. It is visibly noticed that at low temperature, magnitude of Z′ is higher and decreases with rising in frequency, consequently showing a typical negative temperature coefficient of resistance [30]. On increasing both temperature and frequency, Z′ decreases, which confirmed that electrical conductivity increases [31,32]. At all temperatures values, assimilation of Z′ in high frequency region indicate the reduction of barier properties [33,34]. The falling nature of Z′ with

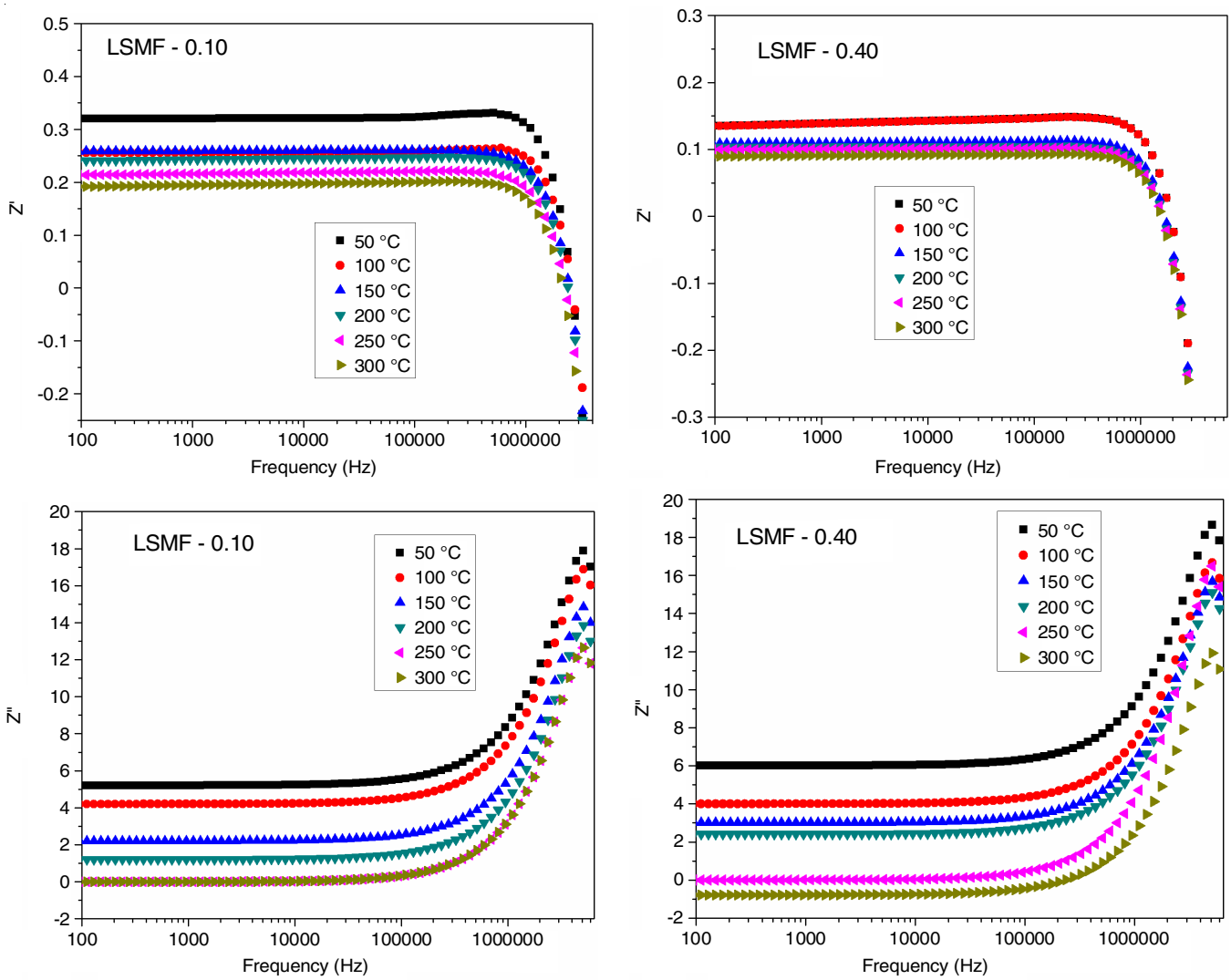

Fig. 7. Z′ and Z″ with respect to frequency response of $La_{1-x}Sr_xMn_{0.50}Fe_{0.50}O_3$ ($x = 0.10$ and 0.40) solid solutions

raise in temperature as well as frequency indicate the reduction of the resistive properties of the prepared material. In all the prepared samples with increasing temperature, broading of peaks is observed which verified the temperature dependent electrical relaxation phenomenon. In higher frequency region, curves of Z′ assimilation proved the disappearnce of space charge polarization [35,36].

Electrical properties: The electric conductivity of the material is given by $G\left(\frac{l}{A}\right) = \sigma_{ac}$, where σ_{ac}, A, *l* and G be the AC conductivity, area of cross-section, thickness of pellet and conductance, respectively. Variation of electrical conductivity with respect to temperature at 25 ºC to 800 ºC of $La_{1-x}Sr_xMn_{0.50}Fe_{0.50}O_3$; ($0.10 \le x \le 0.40$) solid solutions are shown in Fig. 8.

Value of conductivity continually increases with temperature of all the samples. Universal power law (eqn. 5) is used to determine the conductivity of the material.

$$\sigma_{ac} = \omega \varepsilon_0 \varepsilon''(\omega) = \omega \varepsilon_0 \varepsilon'(\omega) \text{ Tan } \delta$$

where ω, ε_0 and tan δ represent as the angular frequency, permittivity in free space and dielectric loss, respectively .The maximum value of the conductivity is given in Table-4 and it is confirmed that replacement of La by Sr increases the conductivity in the material. Substitution of Sr create charge imbalance in the material, which is further compensated by oxidation or reduction of Mn and Fe leads to increases the conductivity of the material. In addition to this as reported in literature, grain, grain boundaries and defects in crystal also play an important role to increase the conductivity. Doping of alkaline earth metals in materials leads to formation of ordered oxygen vacancies clusters, which further act as nucleating sites and therefore make them unavailable for conduction [37,38]. At low temperature, in order to dissociate these clusters and make them to mobile, sufficient energy is required. Therefore, activation energy is the totaling of dissociation energy in addition to migration energy. However, at high temperatures, energy required only for mobile the ions. Consequently overall activation energy is related only to migration energy at high temperature and therefore, at high temperature activation energy value is small as compare to value at low temperature [39,40]. The activation energy (E_a) of the prepared material is determined by the Arrhenius fitting of conductivity with temperature of $La_{1-x}Sr_xMn_{0.50}Fe_{0.50}O_3$; ($0.10 \le x \le 0.40$) solid solutions (Fig. 8), which clearly show that Sr doping decrease the E_a value (Table-4). Thus, the results confirmed that activation energy is in well agreement with conductivity values.

TABLE-4
CONDUCTIVITY AND ACTIVATION ENERGY
OF $La_{1-x}Sr_xMn_{0.50}Fe_{0.50}O_3$ ($0.10 \le x \le 0.40$)

Composition	Conductivity (S cm^{-1})		Activation energy (eV)
	600 °C	800 °C	
$La_{0.90}Sr_{0.10}Mn_{0.50}Fe_{0.50}O_3$	121.09	303.59	0.177
$La_{0.80}Sr_{0.20}Mn_{0.50}Fe_{0.50}O_3$	132.12	328.61	0.164
$La_{0.70}Sr_{0.30}Mn_{0.50}Fe_{0.50}O_3$	149.90	359.93	0.100
$La_{0.60}Sr_{0.40}Mn_{0.50}Fe_{0.50}O_3$	155.96	362.35	0.091

Conclusion

Solid state reaction method was used to prepare $La_{1-x}Sr_xMn_{0.50}Fe_{0.50}O_3$; ($0.10 \le x \le 0.40$) perovskite ceramics bulk material. The XRD analysis confirmed the single phase of the material and rhombohedral crystal structure. The prepared material was well sintered as indicatred by SEM micrographs and the non-uniform grain were randomely oriented whose size decreased as the Sr content increases. Density of the material also decreased with Sr substitution, which is in well agreement with SEM results.TGA analysis showed the weight gain in the the prepared material above 300 ºC. Thermal expansion coefficient (TEC) decreases with Sr substitution. Dielectric analysis confirmed that samples obey non-Debye relaxation behaviour. Conductivity value increases with temperature and Sr substitution. Activation energy was found to be decreased with replacement of La by Sr which is in well agreement with conductivity values. Therefore, it is concluded that the prepared material is recommended to be used as cathode of intermediate temperature solid oxide fuel cells (SOFCs).

CONFLICT OF INTEREST

The authors declare that there is no conflict of interests regarding the publication of this article.

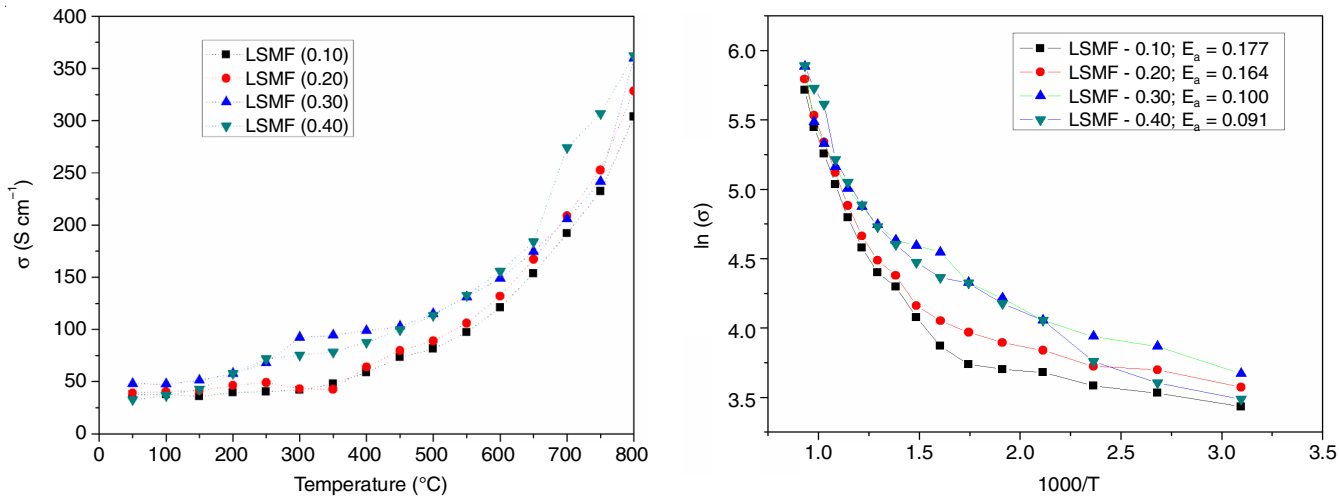

Fig. 8. Conductivity and activation energy *vs.* temperature of $La_{1-x}Sr_xMn_{0.50}Fe_{0.50}O_3$ ($0.10 \le x \le 0.40$)

REFERENCES

1. J.E. O'Brien, C.M. Stoots, J.S. Herring and J. Hartvigsen, *J. Fuel Cell Sci. Technol.*, **3**, 213 (2006); https://doi.org/10.1115/1.2179435
2. A. Hauch, S.H. Jensen, S. Ramousse and M. Mogensen, *J. Electrochem. Soc.*, **153**, A1741 (2006); https://doi.org/10.1149/1.2216562
3. R. Rivera-Tinoco, C. Mansilla and C. Bouallou, *Energy Convers. Manage.*, **51**, 2623 (2010); https://doi.org/10.1016/j.enconman.2010.05.028
4. C. Sun, R. Hui and J. Roller, *J. Solid State Electrochem.*, **14**, 1125 (2010); https://doi.org/10.1007/s10008-009-0932-0
5. C.W. Sun and U. Stimming, *J. Power Sources*, **171**, 247 (2007); https://doi.org/10.1016/j.jpowsour.2007.06.086
6. S.C. Singhal and K. Kendall, High Temperature Solid Oxide Fuel Cells: Fundamentals, Design and Applications, Elsevier: Oxford, pp 1-22 (2003).
7. M. Mogensen and K. Kammer, *Annu. Rev. Mater. Res.*, **33**, 321 (2003); https://doi.org/10.1146/annurev.matsci.33.022802.092713
8. S.C. Singhal, *Solid State Ion.*, **135**, 305 (2000); https://doi.org/10.1016/S0167-2738(00)00452-5
9. M. Dokiya, *Solid State Ion.*, **152-153**, 383 (2002); https://doi.org/10.1016/S0167-2738(02)00345-4
10. N.P. Brandon, S. Skinner and B.C.H. Steele, *Annu. Rev. Mater. Res.*, **33**, 183 (2003); https://doi.org/10.1146/annurev.matsci.33.022802.094122
11. K. Wincewicz and J. Cooper, *J. Power Sources*, **140**, 280 (2005); https://doi.org/10.1016/j.jpowsour.2004.08.032
12. P. Plonczak, M. Gazda, B. Kusz and P. Jasinski, *J. Power Sources*, **181**, 1 (2008); https://doi.org/10.1016/j.jpowsour.2007.12.019
13. J.M. Ralph, A.C. Schoeler and M. Krumpelt, *J. Mater. Sci.*, **36**, 1161 (2001); https://doi.org/10.1023/A:1004881825710
14. N.A. Baharuddin, A. Muchtar and M.R. Somalu, *Int. J. Hydrogen Energy*, **42**, 9149 (2017); https://doi.org/10.1016/j.ijhydene.2016.04.097
15. J.M. Ralph, C. Rossignol and R.J. Kumar, *Electrochem Soc.*, **150**, A1518 (2003); https://doi.org/10.1149/1.1617300
16. S.P. Simner, J.F. Bonnett, N.L. Canfield, K.D. Meinhardt, V.L. Sprenkle and J.W. Stevenson, *Electrochem. Solid-State Lett.*, **5**, A173 (2002); https://doi.org/10.1149/1.1483156
17. S.P. Simner, J.F. Bonnett, N.L. Canfield, K.D. Meinhardt, J.P. Shelton, V.L. Sprenkle and J.W. Stevenson, *J. Power Sources*, **113**, 1 (2003); https://doi.org/10.1016/S0378-7753(02)00455-X
18. G.L. Yuan, S.W. Or and H.L.W. Chan, *J. Phys. D Appl. Phys.*, **40**, 1196 (2007); https://doi.org/10.1088/0022-3727/40/4/043
19. K.J. Park, C.H. Kim, Y.J. Yoon, S.M. Song, Y.T. Kim and K.H. Hur, *J. Eur. Ceram. Soc.*, **29**, 1735 (2009); https://doi.org/10.1016/j.jeurceramsoc.2008.10.021
20. J. Richter, P. Holtappels, T. Graule and L. Gauckler, *Solid State Ion.*, **179**, 2284 (2008); https://doi.org/10.1016/j.ssi.2008.08.007
21. F. Chen, O.T. Sorensen, G. Meng and D. Peng, *J. Mater. Chem.*, **7**, 481 (1997); https://doi.org/10.1039/a605377g
22. A. Weber and E. Ivers-Tiffee, *J. Power Sources*, **127**, 273 (2004); https://doi.org/10.1016/j.jpowsour.2003.09.024
23. W.X. Chen, T.L. Wen, H.W. Nie and R. Zheng, *Mater. Res. Bull.*, **38**, 1319 (2003); https://doi.org/10.1016/S0025-5408(03)00143-0
24. D. Bahadur, W. Fischer and M.V. Rane, *Mater. Sci. Eng. A*, **252**, 109 (1998); https://doi.org/10.1016/S0921-5093(98)00653-4
25. K.S. Cole and H. Robert, *J. Chem. Phys.*, **9**, 341 (1941); https://doi.org/10.1063/1.1750906
26. M. Kumar and K.L. Yadav, *J. Phys. Condens. Matter*, **91**, 242901 (2007); https://doi.org/10.1063/1.2816118
27. J.L. García-Muñoz, C. Frontera, M.A.G. Aranda, A. Llobet and C. Ritter, *Phys. Rev. B Condens. Matter*, **63**, 064415 (2001); https://doi.org/10.1103/PhysRevB.63.064415
28. M.P. Gutierrez, J. Mira and J. Rivas, *Phys. Lett. A*, **323**, 473 (2004); https://doi.org/10.1016/j.physleta.2004.02.030
29. K.A. Jonscher, *J. Phys. D Appl. Phys.*, **32**, R57 (1999); https://doi.org/10.1088/0022-3727/32/14/201
30. T. Badapanda, S. Sarangi, B. Behera and S. Anwar, *Curr. Appl. Phys.*, **14**, 1192 (2014); https://doi.org/10.1016/j.cap.2014.06.007
31. U. Dash, S. Sahoo, P. Chaudhuri, S.K.S. Parashar and K. Parashar, *J. Adv. Ceramics.*, **3**, 89 (2014); https://doi.org/10.1007/s40145-014-0094-0
32. B. Tiwari and R.N.P. Choudhary, *IEEE Trans. Dielectr. Electr. Insul.*, **17**, 5 (2010); https://doi.org/10.1109/TDEI.2010.5411996
33. B. Tiwari and R.N.P. Choudhary, *J. Alloys Compd.*, **493**, 1 (2010); https://doi.org/10.1016/j.jallcom.2009.11.120
34. H. Singh, A. Kumar and K.L. Yadav, *Mater. Sci. Eng. B*, **176**, 540 (2011); https://doi.org/10.1016/j.mseb.2011.01.010
35. R. Ranjan, R. Kumar, B. Behera and R.N.P. Choudhary, *Physica B*, **404**, 3709 (2009); https://doi.org/10.1016/j.physb.2009.06.113
36. M.R. Biswal, J. Nanda, N.C. Mishra, S. Anwar and A. Mishra, *Adv. Mater. Lett.*, **5**, 531 (2014); https://doi.org/10.5185/amlett.2014.4566
37. I. Kosacki, H.U. Anderson, Y. Mizutani and K. Ukai, *Solid State Ion.*, **152-153**, 431 (2002); https://doi.org/10.1016/S0167-2738(02)00382-X
38. K. Huang, R.S. Tichy and J.B. Goodenough, *J. Am. Ceram. Soc.*, **81**, 2565 (1998); https://doi.org/10.1111/j.1151-2916.1998.tb02662.x
39. J.H. Gong, Y. Li, Z.L. Tang, Y.S. Xie and Z.T. Zhang, *Mater. Chem. Phys.*, **76**, 212 (2002); https://doi.org/10.1016/S0254-0584(01)00522-3
40. M. Kurumada, H. Hara, F. Munakata and E. Iguchi, *Solid State Ion.*, **176**, 245 (2005); https://doi.org/10.1016/j.ssi.2004.08.010